Eur. Phys. J. C (2023) 83:807
https://doi.org/10.1140/epjc/s10052-023-11986-x

THE EUROPEAN PHYSICAL JOURNAL C

Regular Article - Theoretical Physics

On the renormalization of non-polynomial field theories

Andrea Santonocito[1,3,a], **Dario Zappalà**[2,3,b]

[1] Dipartimento di Fisica, Università di Catania, Via S. Sofia 64, 95123 Catania, Italy
[2] INFN, Sezione di Catania, Via S. Sofia 64, 95123 Catania, Italy
[3] Centro Siciliano di Fisica Nucleare e Struttura della Materia, Catania, Italy

Received: 12 July 2023 / Accepted: 28 August 2023 / Published online: 11 September 2023

Abstract A class of scalar models with non-polynomial interaction, which naturally admits an analytical resummation of the series of tadpole diagrams is studied in perturbation theory. In particular, we focus on a model containing only one renormalizable coupling that appear as a multiplicative coefficient of the squared field. A renormalization group analysis of the Green functions of the model shows that these are only approximated solutions of the flow equations, with errors proportional to powers of the coupling, therefore smaller in the region of weak coupling. The final output of the perturbative analysis is that the renormalized model is non-interacting with finite mass and vanishing vertices or, in an effective theory limited by an ultraviolet cut-off, the vertices are suppressed by powers of the inverse cut-off. The relation with some non-polynomial interactions derived long ago, as solutions of the linearized functional renormalization group flow equations, is also discussed.

1 Introduction

The ultraviolet (UV) properties of the four-dimensional scalar quantum field theories are substantially under control thanks to a huge amount of results and indications coming not only from the standard perturbative techniques [1,2], but also from different non-perturbative approaches including formal investigations [3,4], or Montecarlo simulations of lattice theories [5–8], or renormalization group (RG) analysis [9–14], all pointing toward the existence of a single fixed point (FP), the Gaussian FP, which admits only a renormalized free field theory, or equivalently an effective scalar field theory whose validity is limited by an UV cut-off, that shows an interaction strength which grows at larger energy scales up to a Landau-like pole.

Despite this tight scenario, the activity of searching for alternative mechanisms, capable of reshaping the UV structure associated to scalar interactions, has been (and still is) quite active, not only to refine or establish novel non-perturbative techniques on a more formal side, but also to investigate on any possible modification of the high energy picture of all contexts where scalar fields are involved, from the UV completion of the Higgs field in the Standard Model to the effective description of the inflaton field in cosmology [15–30].

An old attempt to renormalize quantum field theory by enlarging the derivative sector of the action through the introduction of additional terms containing higher space-time derivatives of the field, [31–33], was reconsidered more recently both for scalar models that present space and time derivatives in equal number, and for anisotropic models where the number of space derivatives in the action is larger than the time derivatives. This is due to the basic principle that an increase of the number of derivatives raises the power the momentum in the propagator, thus reducing the global degree of divergence of a generic quantum correction diagram.

The renormalization of these models, represented in Euclidean space, can be traced back to the structure of the associated Lifshitz FPs, that may appear if higher derivative terms are present in the action [34–36]. So, for instance, the isotropic case with four space and four time derivatives in four dimensions presents a non-trivial phase structure, with a line of Lifshitz FPs, that shares many properties with the two-dimensional Kosterlitz–Thouless transition [37–42].

However, since the presence of time derivatives of order larger than two leads to the Ostrogradski instability, associated with Hamiltonians unbounded from below which violate unitarity [43], it is preferable to maintain only two time derivatives thus avoiding any problem with unitarity in the UV sector. This point of view leads to the anisotropic

[a] e-mail: andreamariasantonocito@gmail.com
[b] e-mail: dario.zappala@ct.infn.it (corresponding author)

case where only two derivatives are kept in one direction (Euclidean time) and a larger number of derivatives is reserved to the other (space) directions. This scheme was proposed in [44] to make the gravitational action renormalizable, but it is also applied to the study of the UV sector of various field theories [45–53]. In fact, even in anisotropic form, a sufficiently high number of space derivatives improves the UV behavior of the theory to the point of converting a UV unstable Lifshitz point into a stable one.

In the anisotropic framework, the role of tadpole diagrams is crucial as, for a sufficiently large number of space derivatives, only this class of diagrams is UV divergent, which makes the renormalization procedure easier to implement. Moreover, as noticed in [49,52,53], under specific assumptions on the couplings of the theory, it is possible to sum the whole series of tadpole diagrams into a compact form and also to prove that the corresponding theory is asymptotically free. Clearly, this renormalization property of the tadpole diagrams follows from the specific structure of the derivative sector, but it is worthwhile to investigate on the the analogous mechanism for a scalar action with standard derivative sector (i.e. two space and two time derivatives), especially because the summable tadpole diagram series comes from a potential that is non-polynomial in the fields and, in principle, one expects these interactions to be non-renormalizable.

Therefore, in this paper we analyse a scalar toy model with standard derivative sector and non-polynomial interaction, that is representative of a class of models which naturally lead to a summable series of tadpole diagrams, to find out whether the mentioned property could lead to interesting consequences even in this case. It turns out that the sum of the tadpole series is sufficient to guarantee the perturbative renormalizability of such a model, although generating a renormalized free scalar theory.

In addition, it must be recalled that a study of the UV sector of scalar non-polynomial theories in four dimensions was conducted long ago in a different context, namely the Renormalization Group (RG) analysis of the Wilsonian action, and the conclusion was achieved that the differential flow equation, suitably linearized around the Gaussian FP, admits a class of relevant solutions, (i.e. solutions that fall into the the Gaussian FP, when the UV limit of the RG energy scale $k \to \infty$ is taken), in contrast with the well settled picture of the trivial scalar theory [15,17,18]. In addition, these solutions can be expressed in the form of a non-polynomial expansion in powers of the field and, they show many similarities with the toy model here considered.

After some debating [12–25,29], these solutions were considered incorrect because (see [29] for a definite explanation), the assumption of uniform smallness of the solution, which is essential when the linear version of the RG flow equation is considered, is in fact violated, at least at large values of the field and, consequently, their flow is not correctly predicted by the linear RG flow equation and the conclusion that they represent asymptotically free interaction is wrong. Then, a comparison of this RG solution with the toy model here considered is mandatory and we need to analyse the RG flow of the latter and point out the differences with the former.

After introducing the scalar toy model and studying its main properties in perturbation theory in Sect. 2 (and those of similar models in Appendix B), in Sect. 3 we pass to a description of the Halpern–Huang solutions and to an investigation on their limits through a diagrammatic analysis. Then, Sect. 4 we apply the RG machinery to our scalar model and show the level of approximation at which it can be taken as a solution of the full flow equation. In addition, the relation with the solution of [15,18] is discussed. Conclusions are reported in Sect. 5.

2 Non-polynomial toy model in perturbation theory

2.1 Main characteristics of the model

In this section we focus on the particular model, whose Euclidean action in four dimensions, $S_E = \int \mathrm{d}^4x \left(\frac{1}{2}\partial_\mu\phi\ \partial_\mu\phi + V(\phi)\right)$ has the following non-polynomial potential

$$V(\phi) = M^4\left(\frac{g_0\phi^2}{2!M^2} + \frac{g_0^2\phi^4}{4!M^4} + \frac{g_0^3\phi^6}{6!M^6} + \cdots\right) = M^4\left[\cosh\left(\sqrt{g_0}\frac{\phi}{M}\right) - 1\right], \tag{1}$$

where M is a fixed (not subjected to renormalization) mass scale, $g_0 > 0$ is the bare coupling constant and the field independent term is set to zero. The structure of $V(\phi)$ is non-polynomial: it is a series where any even power of the field ϕ is included and the coefficients are arranged in such a way that the sum of the series is a known function, namely the hyperbolic cosine of $\left(\sqrt{g_0}\,\phi/M\right)$. This implies that there is only one independent parameter g_0 (besides M), but the powers of g_0 increase proportionally to the powers of the field ϕ in the various terms of the potential, and this allows us to arrange the diagrams in a perturbative series in powers of g_0. Another peculiar feature is that the only dimensional parameter of Eq. (1) is M^2 and, in particular, the bare square mass of the theory is g_0M^2; as a consequence the dimensional content of any renormalized quantity can be expressed in terms of M.

If we want to compute the quantum corrections of the Green Functions, first we need to determine the degree of divergence of each diagram which is different from the standard results, as in this case we deal with vertices with any possible (even) number of legs. Therefore we introduce the

notation: P = total power of g_0 of a diagram; N = number of legs of a specific vertex; E = number of external lines of a diagram; H = number of internal lines of a diagram; L = number of loops of a diagram; V_N = number of vertices with N legs of a diagram; $V = \sum_{\text{vertices}} V_N$ = total number of vertices of a diagram. The following relations hold:

$$P = \sum_{\text{vertices}} \frac{N}{2}, \quad \sum_{\text{vertices}} N = E + 2H, \quad L = H - V + 1 \tag{2}$$

and we notice that the total power P of each diagram is not just the total number of vertices, but it depends on the specific vertices that enter the diagram itself. By combining the first two equations, we get $P = E/2 + H$ and finally the superficial degree of divergence of a diagram, measured as the resulting power of the momentum cut-off Λ used to regulate the UV divergent integrals, is given by:

$$\mathcal{D}_\Lambda = 2P - E - 4V + 4 \tag{3}$$

in contrast to the standard quartic interaction result, $\mathcal{D}_\Lambda = 4 - E$. Equation (2) indicates that, for a given E-point Green function, at a fixed perturbative order in g_0, i.e. at fixed P, the most divergent contribution comes from the diagrams with minimum V, which clearly correspond to the tadpoles with $V = 1$, and we notice that, due to the presence of the tower of couplings appearing in Eq. (1), diagrams with $V = 1$ could still contain an arbitrary number of tadpoles.

This property can now be exploited when considering the order by order renormalization of the model. We start from the 2-point function which, up to the fourth order in g_0, reads:

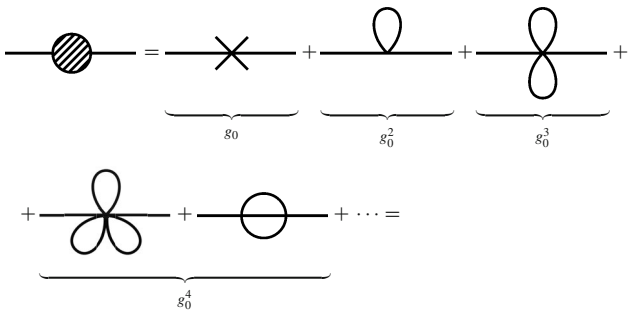

$$= g_0 M^2 + g_0^2\, I + g_0^3\, \frac{1}{2!}\, \frac{I^2}{M^2} + g_0^4 \left(\frac{1}{3!}\, \frac{I^3}{M^4} + S \right) + O(g_0^5) \tag{4}$$

In Eq. (4) the cross indicates the zero-th order vertex and I denotes half of the tadpole integral, which can be computed by means of a four-momentum cut-off Λ

$$I \equiv \quad = \frac{1}{2} \int \frac{d^4k}{(2\pi)^4}\, \frac{1}{k^2 + m^2}$$

$$= c \left(\Lambda^2 - m^2 \log \frac{\Lambda^2}{m^2} \right) \tag{5}$$

where $c = 1/(32\pi^2)$ and m indicates the renormalized mass, while $S(p)$ is the sunset integral with external momentum p:

$$S(p) \equiv$$

$$= \frac{1}{3!} \int \frac{d^4a}{(2\pi)^4} \int \frac{d^4b}{(2\pi)^4}\, \frac{1}{a^2 + m^2}\, \frac{1}{b^2 + m^2} \times \frac{1}{(a + b + p)^2 + m^2} \tag{6}$$

that, with the same regularization, can be written as (see Eq. (A2) in Appendix A)

$$S(p) = \frac{1}{6(4\pi)^2} \left[3\Lambda^2 + p^2 \left(\alpha + \beta \log \frac{\Lambda^2}{m^2} \right) + O\left(\log \frac{\Lambda^2}{m^2} \right) + O(p^2, m^2) \right] \tag{7}$$

with α and β constants. It must be noticed that the most divergent contribution of the tadpole integral is $I_\Lambda \sim \Lambda^2$, as for the sunset integral. Thus, in the fourth order diagrams shown in Eq. (4), the diagram with 3 tadpoles is far more divergent that the sunset and this is just a particular case of the more general property discussed above that, at any given order in perturbation theory, the most divergent diagram is the one with one vertex, namely the one consisting of a product of tadpoles.

Then, in a perturbative scheme, we want to write g_0 as a series expansion of the renormalized coupling g_R:

$$g_0 = g_R + g_R^2\, \delta_1 + \frac{1}{2!} g_R^3\, \delta_2 + \frac{1}{3!}\, g_R^4\, \delta_3 + O(g_R^5) \tag{8}$$

where δ_1, δ_2, δ_3, …are counterterms that must be fixed so that the Green Functions remain finite in the limit $\Lambda \to \infty$. At order $O(g_0)$ we define:

$$\delta_1 = \frac{c}{M^2} \left(\mu^2 - \Lambda^2 - m^2 \log \frac{\mu^2}{\Lambda^2} \right) \tag{9}$$

where μ is a finite arbitrary scale to be fixed by a renormalization condition, so that the dangerous terms when $\Lambda \to \infty$ get cancelled:

$$J(\mu, m^2) = I + \delta_1 M^2 = c \left(\mu^2 - m^2 \log \frac{\mu^2}{m^2} \right) \tag{10}$$

Moreover, at higher order, we choose:

$$\delta_2 = \delta_1^2 - 2\, \delta_1\, \frac{I}{M^2}$$
$$\delta_3 = \delta_1^3 + 6\, \delta_1\, \frac{I^2}{M^4} - 9\, \delta_1^2\, \frac{I}{M^2} - 6\, \frac{S(p^2 = \mu^2)}{M^2} \tag{11}$$

where the external momentum p in Eq. (7) is set equal to the renormalization scale μ and the expansion in Eq. (4) takes

the simple form:

$$= g_R M^2 + g_R^2\, J + g_R^3\, \frac{1}{2!}\, \frac{J^2}{M^2}$$

$$+ g_R^4\, \frac{1}{3!}\, \frac{J^3}{M^4} + O(g_R^5). \tag{12}$$

Then, any divergent term in the limit $\Lambda \to \infty$ is cancelled. With the help of Eq. (11), and by retaining only the most divergent contributions of the integrals I and S, the expansion in Eq. (8) becomes

$$g_0 \sim g_R - g_R^2\, \frac{\Lambda^2}{M^2} + g_R^3\, \frac{3}{2}\, \frac{\Lambda^4}{M^4} - g_R^4 \left(\frac{8}{3}\, \frac{\Lambda^6}{M^6} - 6\, \frac{\Lambda^2}{M^2} \right) \tag{13}$$

and the second term in brackets, coming from the sunset diagram, can be neglected.

Furthermore, if we discard, order by order, all terms with non-leading powers of Λ, we end up with the sum of the multiple tadpole diagrams which, as already discussed, provide at each order, the contribution with the largest power of Λ. This is an essential point. In fact, the various numerical factors of the couplings of the potential in (1) are suitably chosen so that the tadpole series can always be summed to an exponential function as for instance in the case of the six-point vertex:

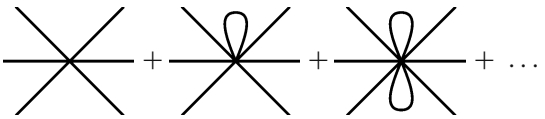

$$= \frac{g_0^3}{M^2}\, e^{g_0 I/M^2}\,. \tag{14}$$

The same holds true for any $2n$-point vertex. Moreover, it is simple to show by induction that any vertex of a generic diagram can be dressed by the exponential tadpole series as indicated below, for instance, for one vertex of the sunset diagram

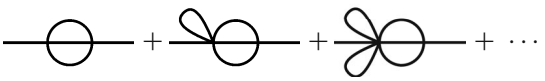

$$= g_0^4\, e^{g_0 I/M^2}\, S \tag{15}$$

Therefore, we shall exploit this property to set a renormalization condition for the coupling g, and we shall check that this is sufficient to fully renormalize the model. The renormalization condition is directly read from the tadpole dressing of the mass term

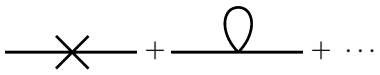

$$= M^2 g_0\, e^{g_0 I/M^2} = M^2 g_R\, e^{g_R J/M^2} \tag{16}$$

i.e. from the following equation that involves both g_0 and the renormalized coupling g_R:

$$g_0\, e^{g_0 I/M^2} = g_R\, e^{g_R J/M^2} \tag{17}$$

It is understood that the right hand side of (17) does not depend on the cut-off Λ and since, according to (10), $J = J(\mu, m^2)$, it follows $g_R = g_R(\mu)$, which guarantees the μ-independence of the left hand side of (17).

Equation (17) has the structure of the Lambert equation $z = we^w$, with complex w and z, that admits a multi-valued solution, made by the branches of the the Lambert function $w_k(z)$ (where k indicates the specific branch). In the case of real w and z, the principal branch of the Lambert function $w_0(z)$ exists only in the range $z \geq 0$ and $-1/e \leq z < 0$, and the large $z \to \infty$ behavior of $w_0(z)$ is

$$w_0(z) \sim \log z - \log\log z \tag{18}$$

If we treat the right hand side of Eq. (17) as a fixed quantity computed at a particular value of μ, and identify $(I/M^2)\, g_0$ with the Lambert function w_0 and also identify $(g_R\, I/M^2)\, \exp\left[g_R\, J/M^2\right]$ with the variable z, we derive the dependence of g_0 on the cutoff Λ directly from (18). In fact, by recalling that $I \sim \Lambda^2$, and defining $\hat{\Lambda}^2 = \Lambda^2/M^2$, we find, for $\hat{\Lambda}^2 \to \infty$,

$$g_0 \sim \frac{\log \hat{\Lambda}^2 - \log\log \hat{\Lambda}^2}{\hat{\Lambda}^2} \tag{19}$$

and it is easy to check that Eq. (19) is consistent with our renormalization condition (17)

$$g_0\, e^{g_0\, I/M^2} = \text{finite} \tag{20}$$

Equation (20) in turn implies: $1/g_0 \sim \exp\left[g_0\, I/M^2\right]$, when $\hat{\Lambda} \to \infty$.

It is worth noticing that also the mass renormalization condition, obtained from the 2-point Green Function by taking the renormalizations scale $\mu = m$,

$$m^2 = M^2\; g_R(m^2)\, e^{g_R(m^2)\, J(m,m^2)/M^2} \tag{21}$$

reduces to a Lambert equation for $g_R(m^2)$, once the two scales m and M are chosen.

2.2 Renormalization to all orders

The next step consists in showing that the renormalization prescription in (17) ensures the cancellation of all divergent

terms. To this purpose we reconsider Eq. (3) where the superficial degree of divergence of a generic diagram is displayed and check how it gets modified when we dress each vertex of the diagram by the full series of tadpoles and, consequently, include the cut-off dependence of g_0 given in Eq. (19).

In other words, we recalculate the degree of divergence of a generic diagram, after inserting the full tadpole series at each vertex of the original diagram and after renormalizing each coupling g_0 according to Eqs. (17) and (19). Then, the diagram shows the following cut-off dependence for $\hat{\Lambda} \to \infty$

$$\left(\frac{\log \hat{\Lambda}^2 - \log\log \hat{\Lambda}^2}{\hat{\Lambda}^2}\right)^{P-V} \hat{\Lambda}^{2P-E-4V+4} = \frac{\left(\log \hat{\Lambda}^2 - \log\log \hat{\Lambda}^2\right)^{P-V}}{\hat{\Lambda}^{E+2V-4}} \tag{22}$$

where the term in brackets in the left hand side comes from the P contributions corresponding to the total count of couplings g_0 of the diagram, minus the number V of vertices, because the tadpole dressing at each vertex transforms one factor g_0 into a $\hat{\Lambda}$-independent, renormalized coupling.

If we neglect the logarithmic corrections in Eq. (22), for any diagram with fixed E and V, the trend for large $\hat{\Lambda}$ is the same, regardless of the form of the specific vertices that enter the diagram itself. This is because any increment by one power of g_0/M^2 in any vertex requires to be compensated, at dimensional level, by a factor Λ^2; however, as $g_0 \sim 1/\hat{\Lambda}^2$, in the end there is no change in the overall trend of the diagram. Logarithmic divergences not taken into account so far, will be analyzed below.

From Eq. (22), it is clear that a larger number of vertices, as well as a larger number of external legs, favours the convergence of the diagram and, as we have already covered (and renormalized) the one-vertex diagrams, the worst possible scenario is represented by the case ($V = 2$, $E = 2$). For this type of diagrams, by neglecting the logarithmic contribution, the cut-off dependence is proportional to $1/\hat{\Lambda}^2$, thus they give zero contribution when the limit $\hat{\Lambda} \to \infty$ is taken. Green functions with larger E and diagrams with $V \geq 2$ have more effective suppressing factor. As a further example, the $O(g_0^9)$ diagram

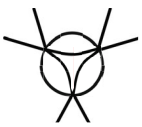

has $\mathcal{D}_\Lambda = 4$ and, after dressing each vertex with the tadpole series and after renormalizing the coupling g_0, we are left with a suppressing factor $g_0^6 \sim 1/\hat{\Lambda}^{12}$. Again, logarithmic corrections have not been taken into account.

However, because of the characteristic $\hat{\Lambda}$ dependence displayed in Eq. (22), the logarithmic corrections within a specific series of diagrams could in principle sum up to a power-like divergent factor, which could potentially lead to an overall divergence. In order to show that this scenario is to be excluded, we concentrate again on the worst possible case. It is easy to realize that the set of diagrams where this effect is maximized, corresponds to the first column in the grid shown below

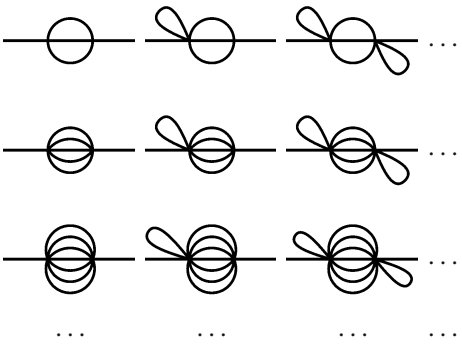

(23)

In fact, along the first column, the sunset diagram on the top-left corner is dressed with the progressive insertion of one internal line that connects the two vertices, thus providing a melonic-like series of diagrams, all with ($V = 2$, $E = 2$) which, according to Eq. (22), gives the largest contribution (apart from the one-vertex diagrams) in the UV limit $\Lambda \hat{\to} \infty$. Then, along each row, at both vertices of the diagram on the left side of the row, we consider the dressing with the tadpole series whose divergent sum is made finite by one power of the coupling g_0, as already shown.

To prove that the full sum of the diagrams in (23) does not produce any dangerous divergence generated by the sum of the logarithmic terms shown in Eq. (22), we proceed by first summing and renormalizing the tadpole series along the rows of (23), and then by making use of the following result, derived in Appendix A in Eq. (A6) (b is a numerical constant),

$$\hat{S} = \quad + \quad + \quad + \cdots \leq g_0^2 I + \frac{bM^4}{I}\left[\cosh\left(g_0 \frac{I}{M^2}\right) - 1 - \frac{1}{2} g_0^2 \frac{I^2}{M^4}\right] \tag{24}$$

i.e. the melonic-like diagram series (where it is understood that the full tadpole series is included to dress each vertex), turns out to be smaller than the right hand side in (24).

It is then straightforward to check that each term of the right hand side in (24) vanishes in the limit $\hat{\Lambda} \to \infty$, according to Eqs. (5) and (19) (note that the $\log\log \hat{\Lambda}^2$ in (19) is essential to compute the correct limit of the hyperbolic cosine). Then, at least in this case, no divergent term is generated by the sum of the logarithmic terms.

Actually, the same series of melonic-like diagrams shows up when computing the 4, 6, 8, 10, ...-point Green func-

tions, even though the series in those cases have different numerical coefficients (generally higher) in front, because of the possible permutations of the external legs. In addition, all possible insertion of different vertices must be counted: for example the 6-point Green function can be constructed with 3 external legs at each of the two vertices, but also with 1 leg in one vertex and 5 legs in the other, and so on. Nevertheless, for these diagrams the suppressing factor is even stronger, because the power of g_0 is higher and because a larger E must be inserted in Eq. (22)). Therefore, all contributions to the $2n$-point Green functions from the melonic-like series in (23) vanish.

Moreover, concerning the $2n$-point Green functions with $n > 1$, there is the contribution of a similar series, see for instance the 4-point Green function

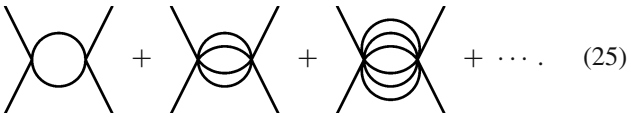

(25)

But, in this case the first diagram of the series is only logarithmically divergent (in contrast to the sunset diagram which is quadratically divergent). So, each diagram of the series is less divergent than the corresponding in (24) and consequently, as in the latter case, we find vanishing contribution. Then, even in the worst-case scenario (namely the 2-point melonic resummation) the logarithmic contributions sum up to a function that is still less divergent than the suppressing powers of $1/\hat{\Lambda}$ coming from the dressed vertices; all other cases are even more suppressed.

Therefore, only the 2-point Green function of this model is finite, due to the tadpole series, while all other Green functions are vanishing: we conclude that the theory is non-interacting, yet it gets a mass renormalization.

Finally, in Appendix B we discuss some models constructed by introducing some modifications with respect to the one in (1), but in all cases considered we end up either with non-renormalizable theories or with structures that are equivalent to the one studied here.

3 RG flow in linear approximation

Now, we reconsider the solutions of the linearized RG flow equation first pointed out in [15,17,18], as they share some crucial properties with the model discussed in Sect. 2. For our purposes, it is sufficient to employ the Wegner–Houghton equation that describes the flow of the running potential $U_k(\phi)$ of a Wilsonian action, in terms of a coarse graining scale k. In fact, as discussed in [29], the linearized equation derived from the Polchinski flow or from the Legendre effective average action flow in the Local Potential approximation, turn our to be equivalent to the previous one.

So, the Wegner–Houghton equation reads:

$$k\partial_k U_k(\phi) = -2ck^4 \log\left(1 + \frac{U_k''(\phi)}{k^2}\right) \tag{26}$$

where $'$ means derivative with respect to the field ϕ. In order to determine the main properties of the flow around the Gaussian FP, it is convenient to re-formulate the equation in terms of dimensionless quantities, obtained by rescaling the dimensional variables in units of the scale k. Therefore we define (k_0 is a boundary value for k)

$$t = \ln\left(\frac{k_0}{k}\right), \quad x = \frac{\phi}{k}, \quad u(t,x) = \frac{U_k(\phi)}{k^4} \tag{27}$$

and, by replacing them in Eq. (26), we get the dimensionless version of the Wegner–Houghton equation. Then, FPs correspond to stationary (i.e. RG time t-independent) solutions $u(x)^*$ of the dimensionless equation. In $d = 4$ the only FP corresponds to the Gaussian solution $u^* = 0$. Finally, in order to determine the eigenvectors associated to the FP, we add to $u(x)^*$ a perturbation proportional to a small parameter δ and to the product of a generic function $w(x)$ and the exponential factor $e^{\lambda t}$ (with real λ):

$$u(x,t) = u(x)^* + w(x)\,\delta\, e^{\lambda t}. \tag{28}$$

With the ansatz in (28) referred to the Gaussian FP $u^* = 0$, the dimensionless Wegner–Houghton equation at linear order in δ, reads

$$\lambda w(x) + x\,\frac{\partial\, w(x)}{\partial x} - 4w(x) = \frac{\partial^2\, w(x)}{\partial x^2} \tag{29}$$

which is a second order, homogeneous linear differential equation for $w(x)$, with eigenvalue λ. By imposing the boundary $\partial_x w|_{x=0} = 0$ associated to the symmetry requirement $w(x) = w(-x)$, and because of the redundancy of the overall normalization of $w(x)$, due to the linearity of the equation, one could expect a unique solution for every value of λ. Then, according to the specific form of $u(t,x)$ in (28), the sign of λ determines whether the eigenmode is relevant ($\lambda > 0$ and solution increasing with t) or irrelevant ($\lambda < 0$ and solution decreasing with t) or marginal ($\lambda = 0$ and no evolution with t).

The direct resolution of Eq. (28), gives a set of solutions with quantised eigenvalues λ and another set with continuously varying λ. They can be summarized by (we shall make use of the notation adopted in [20], and c_0 is an arbitrary normalization)

$$w(x) = c_0\left[1 + \sum_{n=1}^{\infty} \frac{\Pi_{j=1}^{n}(\lambda + 2j - 6)}{(2n)!}\, x^{2n}\right] \tag{30}$$

The quantised spectrum corresponds to $\lambda_h = 4 - 2h$ with $h = 0, 1, 2, 3, \ldots$, that produces a truncation of the infinite sum in (30) and therefore a polynomial solution $w_h(x)$. For each integer value of h, $w_h(x)$ can be expressed in terms of the

orthogonal normalizable basis of the generalised Laguerre polynomials.

On the other hand, any other real value of λ, different from the above integers, gives a non-polynomial infinite sum which can be expressed in terms of the Kummer (confluent hypergeometric) function

$$M\left(\frac{\lambda-4}{2},\frac{1}{2},\frac{x^2}{2}\right). \tag{31}$$

The behavior of (31) with λ not belonging to the quantised spectrum, is exponential at large values of the field $M(a,b,z) \sim e^z/z^{(5-\lambda)/2}$, differently from the polynomial solutions which grow as a power of z. Furthermore, as remarked in [29], due to the exponential behavior of the non-quantised of solutions in (31), these cannot be obtained from an expansion in terms of the the generalised Laguerre polynomials.

As far as quantised polynomial solutions are concerned, it is easy to realize that for $h = 0$ and $h = 1$, one selects respectively a field independent or a quadratic solution in the fields which, as well known, are relevant solutions. Then $h = 2$ is a marginal (at tree level) solution quartic in the field that, due to perturbative corrections, turns out to be irrelevant. Finally all larger values of h represent polynomial irrelevant solutions.

The case of non-quantised solutions is more subtle; in fact, if one selects $\lambda > 0$ (with $\lambda \neq 2$ and $\lambda \neq 4$), the associated Kummer function in (31) is an independent solution (not representable as a linear combination of the quantised polynomials [19]) of the linear equation (29), with positive eigenvalue; therefore it corresponds, in principle, to a relevant eigenmode which allows to take the continuum limit of the corresponding scalar theory, as stated in [18]. However, this conclusion is false as first discussed in [12] and thoroughly explained later in [29]; in fact, the exponential large field behavior of the non-quantised solutions makes the linear approximation adopted in Eq. (29) inadequate at large x^2 and consequently the t evolution of these solutions derived from (29) is in contrast with the one derived from the complete flow equation. Actually, these solutions, at least for large values of x^2, diverge in the UV limit $t \to -\infty$, instead of vanishing as predicted by Eq. (29), [29]. Conversely, the solutions of the quantised spectrum have a much smoother behavior at large x^2, and this implies that both the linear approximation and the full flow equation, predict the same t evolution.

Then, statements on the t evolution (and therefore on the relevance or irrelevance) deduced from Eq. (29) concerning the quantised spectrum, are reliable as they are confirmed at the level of the full flow equation. On the other hand, the t evolution of the solutions with non-quantised spectrum cannot be trusted as it is drastically modified when non-linear effects are taken into account [29].

The solution (30) of the linearized flow equation (29) strongly resembles the potential in (1) and it is natural to apply the perturbative analysis developed in Sect. 2, to these eigenmodes. To this purpose we first need to put back the proper dimensions to the various parameters in (30) and the dimensional potential corresponding to the dimensionless solution in Eq. (28) (for the gaussian FP solution $u^* = 0$), according to Eq. (27), is

$$\begin{aligned} U_k(\phi) &= \delta\, c_0\, k^4 \left(\frac{k}{k_0}\right)^{-\lambda} \\ &\quad\times\left[1+\sum_{n=1}^{\infty}\frac{\Pi_{j=1}^{n}(\lambda+2j-6)}{(2n)!}\left(\frac{\phi}{k}\right)^{2n}\right] \\ &= k_0^4\, h_0(k)\left[1+\sum_{n=1}^{\infty}\frac{h_{2n}(k)}{(2n)!}\left(\frac{\phi}{k_0}\right)^{2n}\right] \end{aligned} \tag{32}$$

where we introduced the couplings

$$h_0(k) = \delta\, c_0 \left(\frac{k}{k_0}\right)^{4-\lambda} \tag{33}$$

$$h_{2n}(k) = \left(\frac{k_0}{k}\right)^{2n} \Pi_{j=1}^{n}(\lambda+2j-6). \tag{34}$$

By identifying k_0 with M in (1), we observe that $U_k(\phi)$ in (32) and $V(\phi)$ in (1) actually have similar structure. However, there are also crucial differences; beside an additional field independent term in (32) which is subtracted away in (1), the couplings in the two expressions have unlike arrangements.

In fact, while in $V(\phi)$ increasing powers of the same coupling appear in front of the various vertices, $U_k(\phi)$ in Eq. (32) is globally proportional to the only coupling $h_0(k)$ that contains undetermined parameters (the product $\delta\, c_0$ and the eigenvalue λ) and the couplings $h_{2n}(k)$, associated to every single vertex, have a well defined structure with no adjustable parameter. In addition, the dependence of $h_0(k)$ and $h_{2n}(k)$ on the scale k is totally determined by the resolution of the linear flow equation. This latter property is essential in the study of the UV properties of $U_k(\phi)$.

If we first focus on the k-dependence of the couplings $h_{2n}(k)$ in Eq. (34), we notice that the powers of $1/k$ precisely compensate the powers of ϕ and the origin of this is the nature of the general solution in Eq. (28), written as the product of two functions, each depending on one of the two dimensionless variables t and x. It is evident that, in the computation of the Green functions, the powers of $1/k$ in the couplings can compensate the divergence of the tadpoles generated by each vertex, and the sum of the tadpole series in each Green function can be computed (note however that it does not sum up to an exponential as e.g. in (14), because of the numerical coefficients in the series).

Therefore for the model (32) with λ real but not integer (otherwise the potential reduces to a polynomial whose renormalization properties are well known), the sum of the tad-

poles contributes to the vacuum fluctuations, 2-, 4-, 6-point Green functions, in the following way:

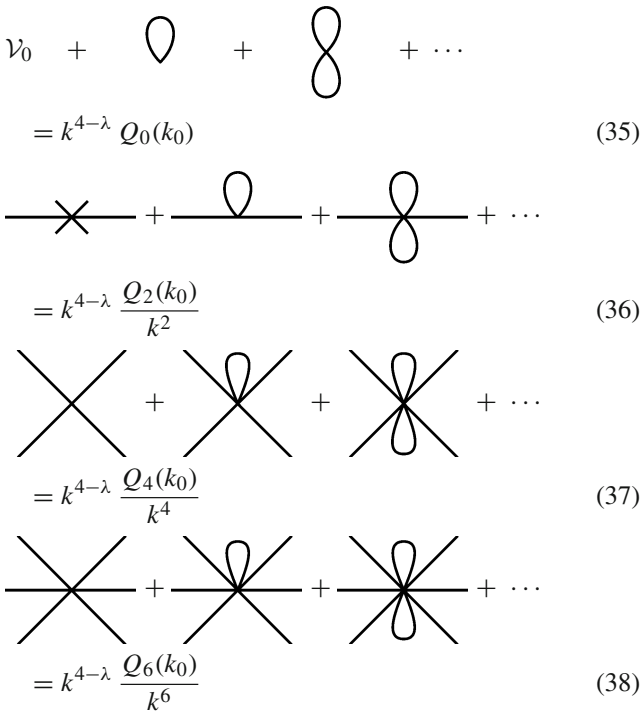

$$= k^{4-\lambda}\, Q_0(k_0) \tag{35}$$

$$= k^{4-\lambda}\, \frac{Q_2(k_0)}{k^2} \tag{36}$$

$$= k^{4-\lambda}\, \frac{Q_4(k_0)}{k^4} \tag{37}$$

$$= k^{4-\lambda}\, \frac{Q_6(k_0)}{k^6} \tag{38}$$

where in the first line $\mathcal{V}_0 = k_0^4\, h_0(k)$ is the zero-th order vacuum contribution from (32), and, in all equations, we factored out the k-dependent part of the sum and identified the UV cut-off Λ of the tadpoles with the running scale k. The common factor $k^{4-\lambda}$ comes from the overall coefficient $h_0(k)$ in Eq. (32) and, finally, $Q_0,\ Q_2,\ Q_4,\ Q_6$ are the k-independent factors resulting from the sum of the tadpoles.

Whether Eqs. (35)–(38) vanish or diverge in the large k limit clearly depends on the eigenvalue λ. In addition, we notice that Eqs. (35)–(38) are indeed representative of the UV behavior of the respective $2n$-point Green functions because, as discussed at length in Sect. 2, all other diagrams containing more than one vertex are subdominant with respect to the tadpole series, because of the suppression factor $O(1/k^{E+2V-4})$ in Eq. (22).

Since integer values of λ, as discussed, correspond to truncated polynomial potentials, whose renormalization properties are well known and do not contain asymptotically free eigenmodes, in the analysis of Eqs. (35)–(38) we focus on non-integer λ. We start with $4 < \lambda$ that, in the limit $k \to \infty$, clearly drives to zero Eqs. (35)–(38) and all higher $2n$-point functions, with increasing powers of $1/k$. If $2 < \lambda < 4$, again all Green functions are vanishing, with the exception of the sum of the vacuum diagrams that instead diverges; no further k-dependent parameter (or, in other words, no further counterterm) is available to cure this divergence. If $0 < \lambda < 2$, even the 2-point function becomes divergent without any possible cure. Further lowering of λ at negative values has the effect of making divergent more and more Green functions.

Then, if we look at the case $\lambda > 0$ which, according to [15,18], corresponds to asymptotically free modes, we find that there is at least one divergent, non-renormalizable, Green function if $\lambda < 4$ (or, by subtracting away from the beginning the vacuum diagrams, the non-renormalizable vertex appears for $\lambda < 2$). Only when $\lambda > 4$ (or $\lambda > 2$ if the vacuum contribution is absent) divergent vertices are avoided, but a suppressing factor in the limit $k \to \infty$, is present in all $2n$-point functions. In the next section we show how this result can be compared to the model in (1).

4 RG approach to the non-polynomial toy model

Before considering the full RG analysis of the model in Eq. (1), we can easily determine the scale dependence of the only parameter which gets renormalized in the scheme developed in Sect. 2, namely the coupling $g_R(\mu)$. In fact, from Eqs. (8) and (9)

$$g_0 = g_R + g_R^2\, \frac{c}{M^2} \left(\mu^2 - \Lambda^2 - m^2 \log \frac{\mu^2}{\Lambda^2} \right) + O(g_R^3) \tag{39}$$

where $c = 1/(32\pi^2)$. Therefore, since g_0 does not depend on the renormalization scale μ, the lowest order β-function of the coupling g_R is

$$\beta_g = \mu\, \frac{\partial g_R}{\partial \mu} = -g_R^2\, \frac{c}{M^2} \left(2\mu^2 - 2m^2 \right) \tag{40}$$

where the last term proportional to m^2 is neglected under the assumption $m^2 << \mu^2$.

Analogous result can be obtained from the full renormalization condition (17), since its left hand side is again μ-independent, and therefore, by neglecting the logarithmic contribution we get

$$\beta_g = -\frac{2c\mu^2 g_R^2}{M^2 + g_R c \mu^2} \tag{41}$$

which, in the lowest order approximation, reproduces Eq. (40). Moreover, these β-functions reproduce as well the dependence of the bare coupling g_0 on the cut-off Λ. We remark that the sign of the β-function in both (40) and (41) is negative.

Incidentally, we mention that the analysis just described has been reconsidered also by using dimensional regularization; in this case however we could not reach the same conclusions because the β-function within this scheme turns out to be different from (41) and we also find inconsistencies as, for instance, the corresponding Lambert equation cannot be solved for positive $\epsilon = 4-d$. This is not unexpected as our model contains an infinite number of dimensional couplings

that can be a source of problems if treated in dimensional regularization, [54]. Therefore, we prefer to retain the regularization procedure based on the use of a UV cut-off that should grasp more accurately the physical content of this specific problem.

Now we turn to a complete RG analysis of the model in (1), by means of the full (not linearized) Wegner-Houghton equation introduced in (26), that in this case reads

$$\frac{M^3\phi\, k\dot{g}(k)}{2\sqrt{g(k)}}\ \sinh\left(\sqrt{g(k)}\frac{\phi}{M}\right) = -2ck^4\log\left[1+\frac{g(k)\,M^2}{k^2}\ \cosh\left(\frac{\phi\sqrt{g(k)}}{M}\right)\right] \tag{42}$$

where we introduced the notation $\dot{g}(k) = dg(k)/dk$.

Equation (42) cannot be solved exactly for $g(k)$. However, by assuming $g(k) << 1$, an approximate solution can be obtained by selecting the coefficients of the various powers of the field ϕ on both sides of the equation or, in other words, by considering the projections of Eq. (42) for the various vertices at zero external momenta. In particular, the flow of the 2-point function at zero momentum is obtained by taking two derivatives with respect to ϕ and setting $\phi = 0$. We get:

$$k\dot{g}(k) = -\frac{2ck^4g^2(k)}{k^2M^2 + M^4g(k)} \tag{43}$$

The resolution of the differential equation to the lowest order gives:

$$g(k) = \frac{g(k_0)}{1+\frac{c}{M^2}\,g(k_0)\left(k^2-k_0^2\right)} \tag{44}$$

where $g(k_0)$ is the value of the coupling constant at the energy scale k_0 and, for large k, we get $\dot{g} \sim -(kg^2)/M^2$ and

$$g \sim \frac{M^2}{k^2} \tag{45}$$

Now, we are able to compare the running coupling found in the perturbative and in the RG approach, namely in Eq. (41) and in Eq. (43). We notice that, despite their agreement at lowest order in g, they differ at higher orders. If we integrate Eq. (41), which was obtained from Eqs. (17), we recover the Lambert function that, as already shown in Eq. (19), for large values of energy goes like (the scale μ is here replaced by k)

$$g_R \sim \frac{\log k^2 - \log\log k^2}{k^2} \tag{46}$$

Conversely, in the RG approach we only get $g \sim 1/k^2$; the logarithmic corrections of the perturbative series are missing and this mismatch is a consequence of the potential in Eq. (1) being an approximate solution of the RG equation, so that the two approaches are compatible only up to these logarithmic terms. Hence, the potential (1) does not identically satisfy the RG flow equation, but at least is a good approximate solution for large values of energy scale (or equivalently for small values of the coupling constant).

Next, we analyze the flow after taking four derivatives with respect to the field in (42) and, to the lowest-order in g, we get

$$g\,\dot{g} = -\frac{ckg^3}{M^2} \tag{47}$$

which, evidently, does not produce the same differential flow equation for g as the one given in Eq. (43). However, if we regard the left hand side of (43) and (47) as the differential flow of the 2- and 4-point Green function respectively (apart from some k-independent constants), we see that the the former is of order $O(g^2)$ from (43), and the latter is $O(g^3)$ from (47). In other words, at large k ($k^2 >> M^2$), the discrepancy between (47) and (43) can be regarded as a higher order effect in g.

Green functions with larger number of external legs produce flow equations that are further suppressed. In fact, for the $2n$-point Green functions at zero external momenta:

$$n\,g^{n-1}\dot{g} = -\frac{2ckg^{n+1}}{M^2} \tag{48}$$

and the suppression factor in the right hand side increases with n. According to the scaling in (45), the $2n$-point functions at large k goes like $\sim (M^{2n}/k^{2n})$.

This result is explanatory in understanding the relation between the potential in (1) and the eigenmodes of the linearized flow equation. In fact, if we use these k-dependent $2n$-point vertices to compute the renormalized sum of the tadpole series displayed in Eqs. (36)–(38) (Eq. (35) is not considered here because in potential (1) the vacuum energy contribution is cancelled out), we recover the result found in Sect. 3 for the specific value $\lambda = 2$ (although it must be recalled that Eqs. (35)–(38) in Sect. 3 require non-integer λ). In other words, the potential in (1) represents a sort of peculiar structure that reproduces the results in Eqs. (36)–(38) for $\lambda = 2$, which instead is not covered by the the eigenmodes of the linearized flow equation. Then, we remark that in Eq. (36) with $\lambda = 2$, any dependence on k is cancelled and we are left with a finite renormalized 2-point function, while Eqs. (37), (38), …depend on inverse powers of k so that they vanish for $k \to \infty$, which corresponds to the findings of Sect. 2, i.e. a renormalized trivial theory with finite mass and vanishing interactions. On the other hand, the same computation with non-integer $\lambda > 2$ yields an unphysical vanishing limit for all relations in (36)–(38) and higher order $2n$-point vertices, i.e. the model with all null renormalized Green functions is meaningless.

Before concluding this paragraph we comment on the physical implications associated to our findings. By taking the point of view of treating the model in (1) as an effective theory with a large but finite physical cut-off k, instead

of ending with a trivial free theory, we can write down an effective potential at the scale k

$$V(\phi) = \frac{1}{2} m_e(k)^2 \phi^2 + \frac{\lambda_e(k)}{4} \phi^4 \tag{49}$$

where higher powers of the field are suppressed by larger inverse powers of the scale k and the effective mass and coupling can be related to the parameters of the original potential in (1) through the RG derived relation in (45),

$$m_e(k)^2 = \frac{M^4}{k^2}, \quad \lambda_e(k) = \frac{M^4}{6\,k^4} \tag{50}$$

By eliminating k in (50), we find

$$M = \frac{m_e(k)}{\sqrt[4]{6\lambda_e(k)}} \tag{51}$$

which generates an effective mass suppression mechanism: because of the interaction effects at large k, we expect a small coupling $\lambda_e(k)$ and consequently a large ratio between the fixed mass and the renormalized effective mass, $M/m_e(k)$. Moreover, the decreasing trend of $\lambda_e(k)$ with k in (50), marks a neat difference, potentially testable, with respect to the scale dependence of the quartic coupling of the standard renormalizable ϕ^4 theory.

5 Conclusions

We analysed a non-polynomial class of scalar potentials that allow to sum the series of tadpole diagrams, as this series contains the most severe UV divergences, and taking care of the latter does guarantee the vanishing of the subleading divergences coming from multiple vertex diagrams. In order to systematically classify the diagrams according to their number of vertices, we adopted a particular toy model that depends on one single renormalizable coupling g_0 in such a way that the potential is an expansion in powers of $g_0\phi^2/M^2$, where M is a fixed mass scale. This naturally allows for a perturbative treatment of the radiative corrections. Despite the infinite tower of non-renormalizable couplings in (1) the perturbative analysis shows that the model is renormalizable, but unfortunately, it is substantially trivial, as only the 2-point Green function at zero external momentum is finite, while all other vertices with at least four external legs vanish in the infinite UV cut-off limit $\Lambda \to \infty$. Although the effect of the interaction modifies the value of the mass scale M into the renormalized mass m, the model is practically indistinguishable from a free theory. Slightly different non-polynomial interactions are also investigated (see Appendix B), but either they are non-renormalizable or, again, reproduce a trivial renormalized theory.

The RG analysis shows a negative β-function of $g(k)$, produced by the scaling of the 2-point function, and we find $g(k) \propto k^{-2}$, rather than $\propto 1/\log(k)$ as e.g. for the non-Abelian Yang–Mills theory. Then, once the flow of $g(k)$ is established, the $2n$-vertices with $n > 1$ proportional to g^n, scale accordingly, i.e. the larger n the stronger the power-like suppression at large k. It must be remarked that the model in (1) is not a full solution of the RG flow, as the numerical coefficient in front of the g^n in each vertex with $n > 1$ (the case $n = 1$ is used to determine the flow of g), is not consistent with the flow equation of that particular vertex. However, due to the increasing power of g with the power of the field in the vertices, one can regard the model as an approximate solution with an error that is suppressed both by the absolute size of $g << 1$ and by the power n of g, characteristic of each vertex.

If, according to the decreasing size of the vertices for increasing n, we consider a two-parameter effective model, valid up to some UV scale k, where all vertices with $n > 2$ are neglected, we find a very weakly interacting theory. However, unlike the two-parameter renormalizable standard ϕ^4 scalar theory, in this case the effective coupling decreases in the UV limit and, potentially, this feature has experimentally testable consequences.

The potentials introduced in [15,18], can be included in our analysis due to the similarities in the form of the non-polynomial interaction which allows to sum the tadpole diagrams. However, the scale dependence of these potentials is entirely established by the resolution of the flow equation, linearized around the Gaussian fixed point. Once these eigenmodes are converted in dimensional form, one finds that each vertex is normalized by the proper inverse power of the running scale k, in addition to an overall factor $k^{4-\lambda}$, exhibiting the eigenvalue λ which establishes the UV properties of the solution.

These solutions cannot be retained as asymptotically free eigenmodes, because they do not respect the linear approximation at large values of the field and consequently the predicted RG-time evolution is wrong, as clearly explained in [29]. The counterpart of these conclusions within our perturbative analysis is that these eigenmodes, depending on the value of λ, are either not renormalizable, because of some residual divergence, or unphysical, because all Green functions are vanishing. Furthermore, these eigenmodes do not include the case of integer λ, while we found that the potential in (1) corresponds to the scaling of Eqs. (35)–(38) with $\lambda = 2$.

Acknowledgements The authors benefited from fruitful discussions with A. Bonanno, V. Branchina, F. Contino. This work has been carried out within the INFN project FLAG.

Data Availability Statement This manuscript has no associated data or the data will not be deposited. [Authors' comment: All data and numerical results concerning the present study are all included in this article.]

Funded by SCOAP[3]. SCOAP[3] supports the goals of the International Year of Basic Sciences for Sustainable Development.

Appendix A

In this appendix we analyze the leading divergence of the sum of the melonic-like diagrams $\hat{S}$, depicted in Eq. (24), in cut-off regularization. First, let us define:

$$\Delta_k = \frac{1}{k^2 + m^2} \tag{A1}$$

Thus, the first integral of the series $\hat{S}$, i.e. the sunset diagram with external momentum p and loop momenta a and b, is given by:

$S(p) \equiv$ 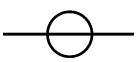 $= \frac{g_0^4}{3!} \int \frac{d^4a}{(2\pi)^4}$

$$\times \int \frac{d^4b}{(2\pi)^4}\, \Delta_a\, \Delta_b\, \Delta_{a+b+p}$$
$$= \frac{g_0^4}{6(4\pi)^2} \left[3\Lambda^2 + p^2 \left(\alpha + \beta \log \frac{\Lambda^2}{m^2} \right) + O\left(\log \frac{\Lambda^2}{m^2} \right) + Q(p,m) \right] \tag{A2}$$

where the result of the integration is taken from [2], and α and β are constants. We will neglect the contribution $O\left(\log \frac{\Lambda^2}{m^2}\right)$ because it is clearly subdominant if compared to Λ^2. In addition, important contributions could come from $Q(p,m)$ when we use the above result for the subsequent diagrams (see below); however it is straightforward to realize that, when $p \sim \Lambda$, the most divergent contribution is proportional to Λ^2:

$$\int \frac{d^4a}{(2\pi)^4} \int \frac{d^4b}{(2\pi)^4}\, \Delta_a\, \Delta_b\, \Delta_{a+b+p} \xrightarrow{p\sim\Lambda} \frac{1}{\Lambda^2} \int \frac{d^4a}{(2\pi)^4} \int \frac{d^4b}{(2\pi)^4} \frac{1}{a^2 b^2} \sim \Lambda^2 \tag{A3}$$

In other words, there is no contribution that goes like $\Lambda^2 \log \frac{\Lambda^2}{m^2}$ and, in the following, we can neglect terms proportional to β in (A2).

Let us now compute the subsequent diagram of the series, this time with external momentum $p = 0$ and with e and f as the additional loop momenta:

 $= \frac{g_0^6}{5!\, M^4} \int \frac{d^4a}{(2\pi)^4} \int \frac{d^4b}{(2\pi)^4} \int \frac{d^4e}{(2\pi)^4}$

$$\times \int \frac{d^4f}{(2\pi)^4}\, \Delta_a\, \Delta_b\, \Delta_e\, \Delta_f\, \Delta_{a+b+e+f}$$
$$= \frac{g_0^6}{5!\, M^4} \int \frac{d^4e}{(2\pi)^4} \int \frac{d^4f}{(2\pi)^4} \left[3!\, S(e+f)\right] \Delta_e\, \Delta_f$$
$$= \frac{g_0^6}{5!\, M^4} \int \frac{d^4e}{(2\pi)^4} \int \frac{d^4f}{(2\pi)^4}\, \Delta_e\, \Delta_f \times \left[\frac{3\Lambda^2}{(4\pi)^2} + \frac{\alpha}{(4\pi)^2} (e+f)^2 \right]$$
$$= \frac{g_0^6}{5!\, M^4} \int \frac{d^4e}{(2\pi)^4} \int \frac{d^4f}{(2\pi)^4}\, \Delta_e\, \Delta_f \times \left[c_1 I + c_2 \left(e^2 + f^2 + 2ef \cos\theta_{ef} \right) \right] \tag{A4}$$

where θ_{ef} is the angle between momenta e and f, I is the tadpole integral already evaluated in Eq. (5), and we defined: $c_1 = 6$ and $c_2 = \alpha/(4\pi)^2$.

By exploiting the symmetry in the last line in Eq. (A4) we find:

 $= \frac{g_0^6}{5!\, M^4} \int \frac{d^4e}{(2\pi)^4}$

$$\times \int \frac{d^4f}{(2\pi)^4}\, \Delta_e\, \Delta_f \left(c_1 I + 2c_2 e^2 \right)$$
$$= \frac{g_0^6}{5!\, M^4} \left(c_1 I^3 + 2c_2 I \int \frac{d^4e}{(2\pi)^4} \frac{e^2}{e^2 + m^2} \right)$$
$$= \frac{g_0^6}{5!\, M^4} \left(c_1 I^3 + 2c_2 I\, c_3 \Lambda^4 \right) = \frac{g_0^6}{5!\, M^4} \left(c_1 I^3 + 2c_2 c_4 I^3 \right)$$

where c_3 and c_4 are constants. By following the same procedure with the successive diagram of the series $\hat{S}$, we get

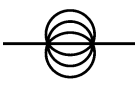 $= \frac{g_0^8}{7!\, M^8} \left(c_1 I^5 + 4c_2 c_4 I^5 \right)$ (A5)

and so on and so forth for all the other diagrams of the series.

Before adding everything up, we have to remember that each vertex must be "dressed" with the tadpole diagrams sum, and this means that a global factor g_0^2 (a factor g_0 for each vertex) must be discarded from the global count of the

powers of Λ in each diagram of $\hat{S}$. Then, the sum reads

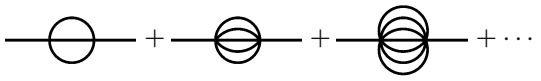

$$
\begin{aligned}
&\sim g_0^2 I + \frac{g_0^4}{5!\,M^4}\,(c_1+2c_2c_4)\,I^3 + \frac{g_0^6}{7!\,M^8}\,(c_1+4c_2c_4)\,I^5 + \cdots \\
&= g_0^2 I + c_1\left(\frac{g_0^4}{5!\,M^4} I^3 + \frac{g_0^6}{7!\,M^8} I^5 + \cdots\right) \\
&\quad + c_2c_4\left(\frac{2}{5!\,M^4} g_0^4 I^3 + \frac{4}{7!\,M^8} g_0^6 I^5 + \cdots\right) \\
&< g_0^2 I + \frac{c_1,\,M^4}{I}\left(\frac{g_0^4 I^4}{4!\,M^8} + \frac{g_0^6 I^6}{6!\,M^{12}} + \cdots\right) \\
&\quad + \frac{c_2c_4\,M^4}{I}\left(\frac{g_0^4 I^4}{4!\,M^8} + \frac{g_0^6 I^6}{6!\,M^{12}} + \cdots\right) \\
&= g_0^2 I + \frac{b\,M^4}{I}\left[\cosh\left(\frac{g_0 I}{M^2}\right) - 1 - \frac{g_0^2 I^2}{2\,M^2}\right]
\end{aligned}
\tag{A6}
$$

where in the last step we have defined $b = c_1 + c_2c_4$. The inequality derived in Eq. (A6) is the one reported in Eq. (24).

Appendix B

In principle, the potential studied in Sect. 2 can be modified to adjust its UV behavior with the aim of obtaining a significant interacting theory. Unfortunately, in all cases here analyzed, the resulting model turns out to be either not practicable or equivalent to the original one and, below, we discuss a few representative cases.

Actually, one of these models is already considered in Sect. 3. It is the one coming from the direct resolution of the RG flow equation, suitably linearized around the Gaussian fixed point, that can be expressed as an expansion in powers of the field but with a rather different structure of the couplings.

Another model, alternative to (1), but very similar in structure, is given by

$$
\begin{aligned}
V(\phi) &= \frac{M^4}{g_0}\left(\frac{g_0\phi^2}{2!M^2} + \frac{g_0^2\phi^4}{4!M^4} + \frac{g_0^3\phi^6}{6!M^6} + \ldots\right) \\
&= \frac{M^4}{g_0}\left[\cosh\left(\sqrt{g_0}\frac{\phi}{M}\right) - 1\right]
\end{aligned}
\tag{B1}
$$

where, as in (1), we do not renormalize the parameter M (i.e. it contains no counterterms), and the only renormalizable parameter is g_0, so that the only difference with respect to the original model is an overall rescaling of the factor $1/g_0$. Then, by repeating the same analysis of Sect. 2, we immediately realize that the sum of the tadpoles (the most divergent diagrams), in the two point function yields $M^2\,e^{g_0 I/M^2}$, which is equal to the result in (16), up to the mentioned rescaling of $1/g_0$ and the same result holds for all $2n$-point Green functions. It is clear that the renormalization condition adopted in Sect. 2 in this case would be insufficient to make the 2-point Green function finite and we need a different prescription. In particular, if we take

$$
M^2 e^{g_0 I/M^2} = M^2 e^{g_R c\mu^2/M^2} \implies e^{g_0 I/M^2} = e^{g_R c\mu^2/M^2}
\tag{B2}
$$

we find the quite simple dependence of g_0 on the UV cut-off Λ

$$
g_0(\Lambda) = g_R\,\frac{\mu^2}{\Lambda^2}
\tag{B3}
$$

which is the same as the one found in Eq. (19), apart from the logarithmic corrections. However, the result in (B3) means that it is not possible to frame this renormalization scheme within the standard series expansion of g_0 in powers of g_R; in other words, here we do not have the usual cancellation of the divergence through the subtraction of an equally divergent counterterm, and we are forced to adopt a multiplicative cancellation.

By following the same power counting analysis performed in Sect. 2, we find that the relation displayed in (B3), leaves finite the sum of the tadpole series in the 2-point Green function and forces to zero all the subleading non-tadpole diagrams. In addition, the tadpole series contributing to all other $2n$-point functions identically vanishes, because of further suppressing multiplicative powers of g_0; as a consequence all but the 2-point Green function are null. Then, we conclude that the renormalized model (B1) is identical to the renormalized (1), although the latter admits a perturbative treatment in terms of counterterms which cannot be applied to the former.

A different approach to the renormalization of this kind of models is instead obtained by allowing for the renormalization of the other parameter appearing in the potential, namely M. So, for instance, we can reconsider the previous case but with the substitution $M \to M_0$, i.e. a bare mass that undergoes renormalization:

$$
\begin{aligned}
V(\phi) &= \frac{M_0^4}{g_0}\left(\frac{g_0\phi^2}{2!M_0^2} + \frac{g_0^2\phi^4}{4!M_0^4} + \frac{g_0^3\phi^6}{6!M_0^6} + \cdots\right) \\
&= \frac{M_0^4}{g_0}\left[\cosh\left(\sqrt{g_0}\frac{\phi}{M_0}\right) - 1\right]
\end{aligned}
\tag{B4}
$$

Of course, the sum of the tadpoles discussed in the previous case still holds, but now we find the ratio g_0/M_0^2 instead of g_0/M^2 in the exponent.

If we now look at the output of the tadpole sum in the 2-point and 4-point functions we get $M_0^2 e^{g_0 I/M_0^2}$ and $g_0 e^{g_0 I/M_0^2}$ respectively. These results are both finite only if the same

counterterms are taken for g_0 and M_0^2. Then, these counterterms get cancelled in the ratio g_0/M_0^2 but they can be chosen in such a way that the tadpole series in the 2-point and 4-point functions is finite. In this case however, we also find that the tadpole series remains finite in any $2n$-point function, as for instance in the 6-point function

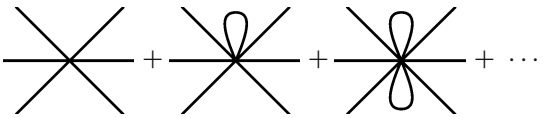

$$= \frac{g_0^2}{M_0^2}\, e^{g_0 I/M_0^2} = \underbrace{\frac{g_0}{M_0^2}}_{\text{finite}}\ \underbrace{g_0\, e^{g_0 I/M_0^2}}_{\text{finite}} \tag{B5}$$

This, in turn, implies that any 2-vertex diagram (like for instance the sunset diagram) with the tadpole series summed at each vertex, produces a divergence that cannot be cured because all counterterms coming from g_0 and M_0^2 have already been used.

We notice that even considering the possibility of renormalizing the mass term M_0 in the original potential in (1), i.e.

$$\begin{aligned} V(\phi) &= M_0^4 \left(\frac{g_0\phi^2}{2!M_0^2} + \frac{g_0^2\phi^4}{4!M_0^4} + \frac{g_0^3\phi^6}{6!M_0^6} + \cdots \right) \\ &= M_0^4 \left[\cosh\left(\sqrt{g_0}\frac{\phi}{M_0} \right) - 1 \right] \end{aligned} \tag{B6}$$

we would get $g_0\, M_0^2 e^{g_0 I/M_0^2}$ and $g_0^2 e^{g_0 I/M_0^2}$ as output of the tadpole sum in the 2-point and 4-point functions and consequently, as before, the same renormalization counterterms for g_0 and M_0^2 are required. Then, the same flaw encountered in the previous example shows up even in this case, namely the requirement to fix the counterterms by imposing a finite tadpole series, implies as well the presence of uncured divergences in the diagrams containing at least two vertices, such as the sunset diagram.

References

1. S. Coleman, R. Jackiw, H.D. Politzer, Spontaneous symmetry breaking in the O(N) model for large N. Phys. Rev. D **10**, 2491 (1974)
2. J. Iliopoulos, C. Itzykson, A. Martin, Functional methods and perturbation theory. Rev. Mod. Phys. **47**, 165 (1975)
3. M. Aizenmann, Proof of the triviality of ϕ_d^4 field theory and some mean-field features of Ising models for $d>4$. Phys. Rev. Lett. **47**, 1 (1981)
4. J. Frohlich, On the triviality of ϕ_d^4 theories and the approach to the critical point in $d \geq 4$ dimensions. Nucl. Phys. B **200**, 281 (1982)
5. M. Luscher, P. Weisz, Scaling laws and triviality bounds in the lattice ϕ^4 theory. 1. One component model in the symmetric phase. Nucl. Phys. B **290**, 25 (1987)
6. M. Luscher, P. Weisz, Scaling laws and triviality bounds in the lattice ϕ^4 theory. 2. One component model in the phase with spontaneous symmetry breaking. Nucl. Phys. B **295**, 65 (1988)
7. M. Luscher, P. Weisz, Scaling laws and triviality bounds in the lattice ϕ^4 theory. 3. N component model. Nucl. Phys. B **318**, 705 (1989)
8. A. Hasenfratz, K. Jansen, J. Jersak, C.B. Lang, T. Neuhaus, H. Yoneyama, Study of the four component phi**4 model. Nucl. Phys. B **317**, 81 (1989)
9. K.G. Wilson, J.B. Kogut, The renormalization group and the epsilon expansion. Phys. Rep. **12**, 75 (1974)
10. A. Hasenfratz, P. Hasenfratz, Renormalization group study of scalar field theories. Nucl. Phys. B **270**, 687 (1986)
11. J. Zinn-Justin, *Quantum Field Theory and Critical Phenomena* (Clarendon Press, Oxford, 1990)
12. T.R. Morris, Comment on"fixed-point structure of scalar fields". Phys. Rev. Lett. **77**, 1658 (1996)
13. T.R. Morris, Three-dimensional massive scalar field theory and the derivative expansion of the renormalization group. Nucl. Phys. B **495**, 477 (1997). arXiv:hep-th/9612117
14. T.R. Morris, Elements of the continuous renormalization group. Prog. Theor. Phys. Suppl. **131**, 395 (1998). arXiv:hep-th/9802039
15. K. Halpern, K. Huang, Fixed-point structure of scalar fields. Phys. Rev. Lett. **74**, 3526 (1995)
16. V. Periwal, Halpern–Huang directions in effective scalar field theory. Mod. Phys. Lett. A **11**, 2915 (1996). arXiv:hep-th/9512108
17. K. Halpern, K. Huang, Halpern and Huang reply. Phys. Rev. Lett. **77**, 1659 (1996)
18. K. Halpern, K. Huang, Nontrivial directions for scalar fields. Phys. Rev. D **53**, 3252 (1996)
19. A. Bonanno, Nonperturbative scaling in the scalar theory. Phys. Rev. D **62**, 027701 (2000). arXiv:hep-th/0001060
20. V. Branchina, Nonperturbative renormalization group potentials and quintessence. Phys. Rev. D **64**, 043513 (2001). arXiv:hep-ph/0002013
21. H. Gies, Flow equation for Halpern–Huang directions of scalar o(n) models. Phys. Rev. D **63**, 065011 (2001). arXiv:hep-th/0009041
22. B. Altschul, Nonpolynomial normal modes of the renormalization group in the presence of a constant vector potential background. Nucl. Phys. B **B705**, 593 (2005). arXiv:hep-th/0403093
23. B. Altschul, V.A. Kostelecky, Spontaneous Lorentz violation and nonpolynomial interactions. Phys. Lett. B **628**, 106 (2005). arXiv:hep-th/0509068
24. H. Gies, M.M. Scherer, Asymptotic safety of simple Yukawa systems. Eur. Phys. J. C **66**, 387 (2010). arXiv:0901.2459
25. A.R. Pietrykowski, Interacting scalar fields in the context of effective quantum gravity. Phys. Rev. D **87**, 024026 (2013). arXiv:1210.0507
26. B. Holdom, J. Ren, C. Zhang, Stable asymptotically free extensions (SAFEs) of the standard model. JHEP **03**, 028 (2015). arXiv:1412.5540
27. H. Gies, L. Zambelli, Asymptotically free scaling solutions in non-Abelian Higgs models. Phys. Rev. D **92**, 025016 (2015). arXiv:1502.05907
28. H. Gies, L. Zambelli, Non-Abelian Higgs models: paving the way for asymptotic freedom. Phys. Rev. D **96**, 025003 (2017). arXiv:1611.09147
29. I. Hamzaan Bridle, T.R. Morris, Fate of nonpolynomial interactions in scalar field theory. Phys. Rev. D **94**, 065040 (2016). arXiv:1605.06075
30. T.R. Morris, Properties of the linearized functional renormalization group. Phys. Rev. D **105**, 105021 (2022). arXiv:2203.01195
31. W. Thirring, Regularization as a consequence of higher order equations. Phys. Rev. **77**, 570 (1950)
32. A. Pais, G.E. Uhlenbeck, On field theories with nonlocalized action. Phys. Rev. **79**, 145 (1950)

33. K.S. Stelle, Renormalization of higher derivative quantum gravity. Phys. Rev. D **16**, 953 (1977)
34. R. Hornreich, M. Luban, S. Shtrikman, Critical behavior at the onset of k-space instability on the λ line. Phys. Rev. Lett. **35**, 1678 (1975)
35. R.M. Hornreich, The Lifshitz point: phase diagrams and critical behavior. J. Magn. Magn. Mater. **15**, 387 (1980)
36. H. Diehl, M. Shpot, Critical, crossover, and correction to scaling exponents for isotropic Lifshitz points to order $(8-d)^2$. J. Phys. A **35**, 6249 (2002). arXiv:cond-mat/0204267
37. A. Bonanno, D. Zappala, Isotropic Lifshitz critical behavior from the functional renormalization group. Nucl. Phys. B **893**, 501 (2015). arXiv:1412.7046
38. D. Zappala, Isotropic Lifshitz point in the O(N) theory. Phys. Lett. B **773**, 213 (2017). arXiv:1703.00791
39. D. Zappala, Indications of isotropic Lifshitz points in four dimensions. Phys. Rev. D **98**, 085005 (2018). arXiv:1806.00043
40. D. Zappala, Isotropic Lifshitz scaling in four dimensions. Int. J. Geom. Methods Mod. Phys. **17**, 2050053 (2020). arXiv:1912.03071
41. N. Defenu, A. Trombettoni, D. Zappala, Topological phase transitions in four dimensions. Nucl. Phys. B **964**, 115295 (2021). arXiv:2003.04909
42. D. Buccio, R. Percacci, Renormalization group flows between Gaussian fixed points. JHEP **10**, 113 (2022). arXiv:2207.10596
43. F.J. de Urries, J. Julve, Ostrogradski formalism for higher derivative scalar field theories. J. Phys. A **31**, 6949 (1998). arXiv:hep-th/9802115
44. P. Horava, Quantum gravity at a Lifshitz point. Phys. Rev. D **79**, 084008 (2009). arXiv:0901.3775
45. D. Anselmi, M. Halat, Renormalization of Lorentz violating theories. Phys. Rev. D **76**, 125011 (2007). arXiv:0707.2480
46. R. Iengo, J.G. Russo, M. Serone, Renormalization group in Lifshitz-type theories. JHEP **11**, 020 (2009). arXiv:0906.3477
47. A. Dhar, G. Mandal, S.R. Wadia, Asymptotically free four-fermi theory in 4 dimensions at the z=3 Lifshitz-like fixed point. arXiv:0905.2928
48. P. Horava, Quantum criticality and Yang–Mills gauge theory. Phys. Lett. B **694**, 172 (2011). arXiv:0811.2217
49. J. Alexandre, Lifshitz-type quantum field theories in particle physics. Int. J. Mod. Phys. A **26**, 4523 (2011). arXiv:1109.5629
50. W. Chao, Horava—Lifshitz type quantum field theory and hierarchy problem. Commun. Theor. Phys. **65**, 743 (2016). arXiv:0911.4709
51. A.R. Solomon, M. Trodden, Higher-derivative operators and effective field theory for general scalar-tensor theories. JCAP **02**, 031 (2018). arXiv:1709.09695
52. D. Zappala, Ultraviolet properties of Lifshitz-type scalar field theories. Eur. Phys. J. C **82**, 341 (2022). arXiv:2111.08385
53. E. Rizza, D. Zappala, Lorentz symmetry violating Lifshitz-type field theories. Mod. Phys. Lett. A **37**, 2250203 (2022). arXiv:2209.11060
54. C. Branchina, V. Branchina, F. Contino, N. Darvishi, Dimensional regularization, Wilsonian RG, and the naturalness and hierarchy problem. Phys. Rev. D **106**, 065007 (2022). arXiv:2204.10582